Available online at www.sciencedirect.com
SCIENCE DIRECT®
International Journal of Heat and Mass Transfer 48 (2005) 3352–3362
International Journal of HEAT and MASS TRANSFER
www.elsevier.com/locate/ijhmt

Gas–liquid mass transfer in a cross-flow hollow fiber module: Analytical model and experimental validation

V.Y. Dindore [a,b,*], G.F. Versteeg [b]

[a] NTNU, Institute for Kjemisk Processteknologi, Sem Sælandsvei 4, N-7491 Trondheim, Norway
[b] Design and Development of Industrial Processes, Chemical Technology, University of Twente, P.O. Box 217, 7500 AE Enschede, The Netherlands

Received 14 July 2004; received in revised form 17 January 2005

Abstract

The cross-flow operation of hollow fiber membrane contactors offers many advantages and is preferred over the parallel-flow contactors for gas–liquid mass transfer operations. However, the analysis of such a cross-flow membrane gas–liquid contactor is complicated due to the change in concentrations of both phases in the direction of flow as well as in the direction perpendicular to flow. In addition, changes in the volumetric flow rate of compressible fluid can also occur over the volume of membrane contactor. These hollow fiber membrane contactors resemble to the more conventional shell and tube cross-flow heat exchanges where a similar variation in the local driving force within the module occurs. Hence heat transfer analogy can be applied to predict the performance of these contactors.

Analytical expressions are derived in this work to describe the mass transfer in these hollow fiber cross-flow contactors analogously to heat transfer in cross-flow shell and tube heat exchangers. CO_2 absorption experiments were carried out in a commercial as well as in the lab-made single-pass cross-flow hollow fiber membrane contactors to check the applicability of this heat transfer analogy under different conditions. Experimental results show that the derived analytical expressions can be applied to the cross-flow membrane gas–liquid contactor under the asymptotic conditions of negligible or small volumetric flow changes. However, in the case of significant changes in the flow rate of compressible fluid, the application of heat transfer analogy results into slight under predictions of the module performance. A more rigorous model is then required for an accurate prediction of the performance.
© 2005 Elsevier Ltd. All rights reserved.

Keywords: Absorption; Mass transfer; Membranes; Membrane contactor; Heat transfer analogy

1. Introduction

The gas–liquid contacting operation is conventionally carried out in direct contact equipment such as packed or bubble columns. These direct contact equipments have many disadvantages like flooding, unloading, emulsion formation, limitation on independent phase flow rate variations and non-linear scale up. Non-dispersive gas–liquid contacting using microporous membranes is an alternative technology that overcomes these disadvantages as well as offers a significantly higher mass transfer area. Such devices are typically referred as 'membrane contactors'. In view of

* Corresponding author. Tel.: +47 73594598; fax: +47 73594080.
E-mail address: vishwas.dindore@chemeng.ntnu.no (V.Y. Dindore).

0017-9310/$ - see front matter © 2005 Elsevier Ltd. All rights reserved.
doi:10.1016/j.ijheatmasstransfer.2005.03.002

Nomenclature

a	dimensionless x-coordinate [–]
A	area [m^2]
b	dimensionless y-coordinate [–]
C	concentration [mol m^{-3}]
D	diffusivity [m^2 s^{-1}]
K	mass transfer coefficient [m s^{-1}]
m	distribution coefficient $(C_L/C_G)_{equilibrium}$ [–]
Q	flow rate [m^3 s^{-1}]
r	fiber radius [m]
V	velocity [m s^{-1}]
W	mass transfer rate [mol s^{-1}]
X	x-dimension of module [–]
Y	y-dimension of module [–]

Greek symbol

Θ	dimensionless concentration

Subscripts

e	exit
G	gas
i	inlet
in	inner
L	liquid
xm	average value

the higher mass transfer area offered by hollow fibers, the modules made using hollow fiber membranes have received wide attention as 'membrane contactors' for industrial applications. The hollow fiber membrane modules can be classified as parallel-flow or cross-flow based on the relative flow directions of the fluids. In general, cross-flow operation of hollow fiber membrane contactors is preferred as it offers several advantages such as higher mass transfer coefficients and lower shell-side pressure drop when compared to the parallel flow contactors. Wickramasinghe et al. [1] evaluated the performance of different parallel and cross-flow gas–liquid membrane contactors based on the equal flow per membrane area and equal flow per module volume and found that in both cases cross-flow membrane modules were more effective as compared to parallel flow modules. Jansen et al. [2] used the cross-flow membrane module made of polypropylene hollow fibers for the reactive absorption of SO_2 and found that mass transfer coefficients for the cross-flow modules were typically one order of magnitude higher than that for conventional parallel flow modules. In addition, the shell-side pressure drop was also found to be considerably lower for the cross-flow modules. This difference in the module performance is mainly due to the flow path taken by the shell-side fluid. In general, the differences in shell-side fluid paths affect module performance in two ways. First, the extent of mass transfer varies from streamline to streamline due to the residence time distribution and channeling of the shell-side fluid. Spread in residence time and channeling effects result in lower mass transfer rates. As the cross-flow contactors have reduced channeling, their performance is comparatively better. Secondly, the local mass transfer resistance is a function of local velocity and turbulence. In the case of cross-flow contactors concentration boundary layer break-up occurs due to continuous splitting and remixing of the shell-side fluid, thus increasing local turbulence level. Hence the mass transfer coefficient obtained in the cross-flow contactors turns out to be higher as compared to the one obtained in parallel flow contactors. However, in the case of the cross-flow membrane contactors the concentrations of both fluids vary in both directions, i.e., in the direction of the flow and in the direction perpendicular to the flow. Hence, unlike parallel flow contactors, simple logarithmic averaging of the concentration driving force cannot be used to predict the performance of the cross-flow contactors. Thus theory of cross-flow membrane contactors turns out to be rather complicated.

These cross-flow hollow fiber membrane modules resemble in operation as well as in construction to the more conventional cross-flow shell and tube heat exchangers. In addition, the local variation in the driving force with position in the both cases is similar. This suggests that mass transfer in these modules can be described analogously to the heat transfer in the cross-flow heat exchangers. However, in the case of cross-flow membrane gas–liquid contactors along with the change in the concentrations, the volumetric flow of the gas phase can also change significantly over the volume of the module. In such cases direct application of the heat transfer analogy may lead to erroneous results. In addition, when mass transfer is enhanced by chemical reaction direct application of heat transfer analogy is not possible. In these situations, the performance of these types of contactors therefore need be analyzed by detailed mathematical modeling. However, in asymptotic case of no or low change in the gas phase flow rate and in the absence of chemical reactions, the heat transfer analogy can be applied to evaluate the performance of a cross-flow membrane gas–liquid contactors.

In the present work, analytical expressions are derived, analogous to the analytic solutions developed for the cross-flow heat exchangers, to describe the mass transfer in the cross-flow hollow fiber modules in

limiting cases. To experimentally validate these derived analytical expressions, CO_2 absorption experiments were carried out in single-pass cross-flow membrane contactors using water as a solvent.

2. Theory

Detailed analysis of a cross-flow heat exchanger and analytical solutions to predict the performance of the cross-flow heat exchanger have been presented by several investigators [3–5]. This literature is mainly focused on the calculation of mean temperature difference in single-pass and multi-pass heat exchangers. Based on this mean temperature difference, the performance of the cross-flow heat exchangers can be predicted accurately. This heat transfer analysis in cross flow heat exchangers can be adapted to describe the mass transfer in cross-flow gas–liquid membrane contactors by making following assumptions;

1. Steady state and isothermal operation.
2. No chemical reaction, only physical mass transfer.
3. The changes in volumetric flow rates are very small and can be neglected.
4. Overall mass transfer coefficient and distribution coefficient are constant over the module.

The cross-flow membrane contactor is shown schematically in Fig. 1. As it can be seen from the figure that the liquid is passed through the fiber and gas is passed through shell side. Thus the fresh liquid meets feed gas at $x = 0$ and $y = 0$. A mass balance for a solute over a small rectangular element of area $\mathrm{d}x\,\mathrm{d}y$, results into two partial differential equations.

$$\frac{\partial C_G}{\partial y} = -\frac{KX}{Q_G}(mC_G - C_L) \tag{1}$$

$$\frac{\partial C_L}{\partial x} = \frac{KY}{Q_L}(mC_G - C_L) \tag{2}$$

where 'm' is the solubility of solute in terms of distribution coefficient and 'K' is the overall mass transfer coefficient. The overall mass transfer coefficient consists of three individual mass transfer coefficients namely; the gaseous phase, the membrane and the liquid phase mass transfer coefficient. In the case of physical absorption of a sparingly soluble solute, the overall mass transfer coefficient can be approximated to the liquid mass transfer coefficient. In the present case liquid is passed through the fiber, hence the overall mass transfer can be given by Graetz–Leveque equation [7].

$$K = 1.62D^{2/3}\left(\frac{V_L}{2Lr_{in}}\right)^{1/3} \tag{3}$$

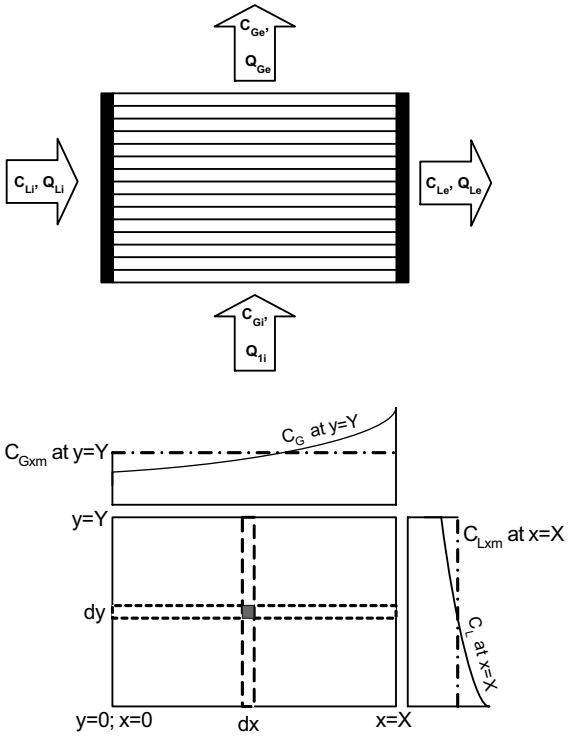

Fig. 1. Cross-flow membrane contactor.

Once the module outlet concentrations '$C_{G,e}$' and '$C_{L,e}$' are known, the overall mass transfer rates can be obtained by

$$W = Q_G(C_{Gi} - C_{Ge}) = Q_L(C_{Le} - C_{Li}) = KA(\Delta C)_{xm} \tag{4}$$

where is 'A' is the overall mass transfer area and $(\Delta C)_{xm}$ is the mean effective concentration difference. It was shown in the earlier study that in the case of rectangular cross-flow hollow fiber membrane modules the shell-side mixing in the direction of flow as well as in the direction perpendicular to the flow is very small and can be neglected [6]. Therefore, in the analysis, both shell side as well as fiber-side fluids were assumed to be unmixed. The exact solution in this case requires simultaneous solving of the differential Eqs. (1) and (2). The complete mathematical derivation is given in Appendix A. The final solutions to calculate the average dimensionless outlet concentrations are given below.

$$\Theta_{G\,xm} = \frac{1}{a^*}\sum_{N=0}^{\infty}\left(1 - e^{-a^*}\sum_{N=0}^{N}\frac{(a^*)^N}{N!}\right) \times \left(1 - e^{-mb^*}\sum_{N=0}^{N}\frac{(mb^*)^N}{N!}\right) \tag{5}$$

$$\Theta_{\mathrm{L\,xm}} = 1 - \frac{1}{mb^*}\sum_{N=0}^{\infty}\left(1 - \mathrm{e}^{-mb^*}\sum_{N=0}^{N}\frac{(mb^*)^N}{N!}\right) \times \left(1 - \mathrm{e}^{-a^*}\sum_{N=0}^{N}\frac{(a^*)^N}{N!}\right) \quad (6)$$

where $\Theta_{\mathrm{G\,xm}}$ and $\Theta_{\mathrm{L\,xm}}$ are the average dimensionless outlet concentrations of gas phase and liquid phase, respectively. a and b are dimensionless x and y coordinates as defined by Eq. (A.1).

3. Experimental

3.1. Material

Double distilled water was used as an absorption solvent. CO_2 and N_2 used in the experiments were of 99.99% purity. Owing to the commercial availability and the high hydrophobic nature of polypropylene as membrane material, it was decided to use an Accurel Q3/2 polypropylene hollow fiber (outside diameter = 1000 μm; wall thickness = 200 μm; maximum pore size = 0.64 μm.) for module construction. The details of the modules used in the experiments are given in Table 1.

Module I was provided by TNO–MEP, Apeldoorn, The Netherlands, and module II was specifically constructed for the present work. The details of the modules are shown in Fig. 2a and b. Both modules had PVC shell housing. Fibers in both modules were arranged in the square pitch. For construction simplicity reason, the shell housing of module II was kept circular with an internal diameter of 5 cm. To make the shell-side flow area rectangular in cross section, a rectangular opening was cut from the circular shell and the concave volume of the shell was filled with epoxy resin. To arrange the fibers uniformly the tube-sheets of the module II were drilled with a 1.2 mm precision drill. The fibers were then woven through the tube sheets. Once all fibers were woven, a liquid epoxy resin (slow setting) was poured on the tube sheet so that the gaps between the fibers are filled. Sufficient time (12 h) was allowed to cure the epoxy. The procedure was repeated until the desired length of the epoxy glue was obtained. The same procedure was used to pot the other end of the module. In both modules the length of the potting was more than 5 cm. This ensures that the potting length on the liquid entry side provides sufficient distance ($>10d_{\mathrm{in}}$) for the laminar liquid flow profile inside the fiber to be fully developed, before it contacts the gas. Uniform flow distribution on the shell-side is important to prevent the maldistribution and dead zones formation. To achieve uniform flow distribution on the shell-side, fluid was passed through an area-reducer filled with glass wool.

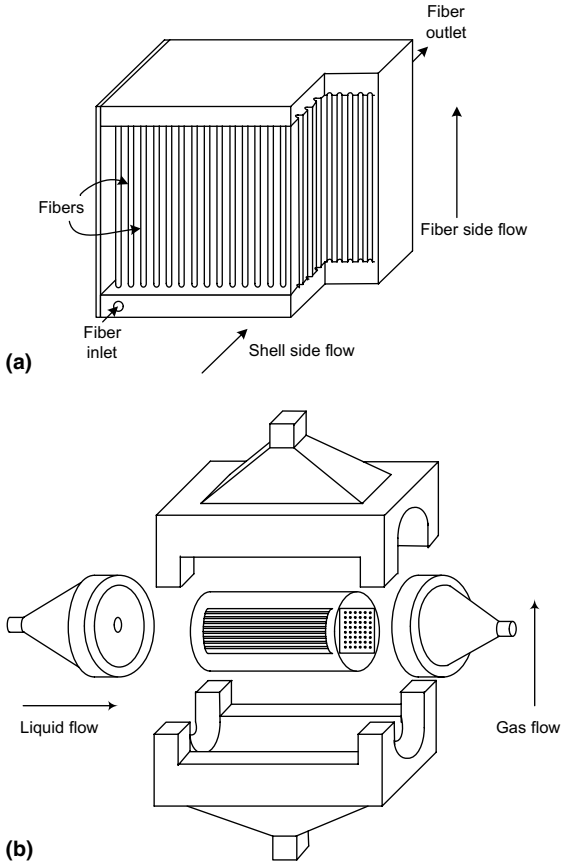

Fig. 2. (a) Cross-flow membrane module I. (b) Cross-flow membrane module II.

3.2. Method

The experimental set-up to study the physical absorption of CO_2 in the cross-flow membrane modules is shown in Fig. 3. A continuous mode of gas–liquid contacting operation with liquid on fiber-side and gas on

Table 1
Module specifications

Module	Fiber type	Length (m)	Width (m)	Height (m)	No. of fibers	Voidage	Pitch	A (m^2)
I	PP	0.1	0.1	0.1	4900	0.615	1.45	0.924
II	PP	0.1	0.04	0.04	400	0.8	2.0	0.074

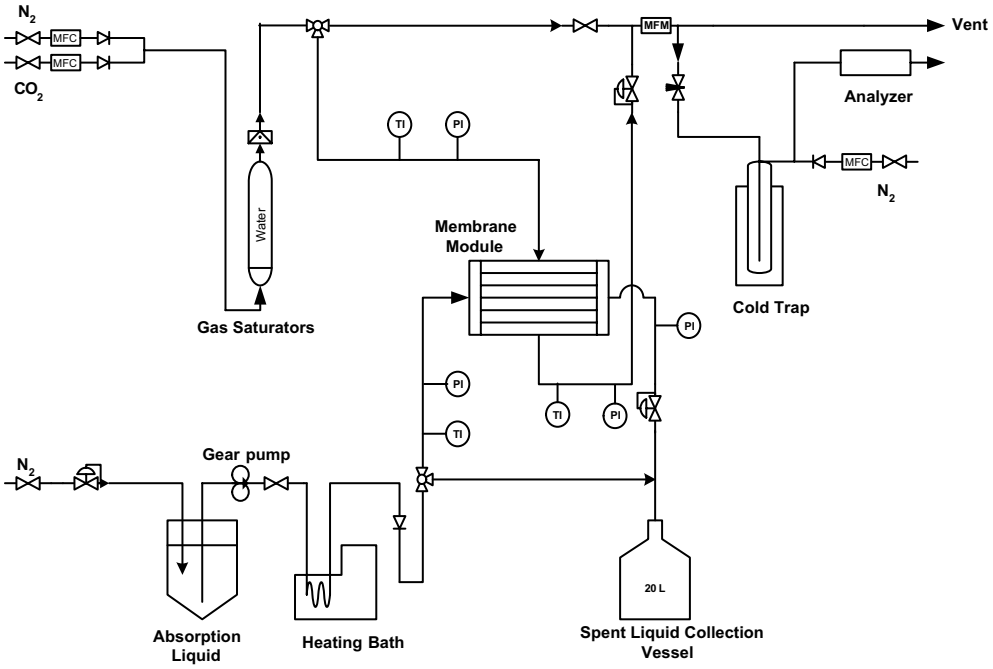

Fig. 3. Cross-flow membrane module experimental set up.

shell side was used during the experiments. The solvent was fed from a gear pressure pump via a flow controller. The solvent used in the experiments was degassed before the usage by N_2 bubbling in a separate apparatus. The solvent was passed through the heat exchanger to maintain the desired temperature before passing to the hollow fiber membrane module. The upstream solvent pressure was controlled using a high-precision back-pressure controller valve. In all experiments, sufficient gas pressure was maintained in the contactor before starting the liquid flow as the absence of the gas pressure may result in the wetting of the fiber. The liquid inlet and liquid outlet pressures were measured separately using digital pressure indicators. The liquid inlet was also fitted with a digital thermometer to monitor the liquid inlet temperature. The average velocity of the liquid through the fibers was measured by weighing a collected amount of sample in a fixed period of time.

The shell-side gas flow was adjusted using calibrated mass-flow controllers. N_2 and CO_2 were premixed to a desired concentration using mass flow controllers and fed to the contactor after saturating the gas stream with water vapor. The shell-side pressure was controlled using a 5866-Brooks digital pressure controller. During all the experiments the liquid-side pressure was kept higher than the shell-side gas pressure to avoid the bubbling of gas. The gas inlet and outlet pressure were measured separately using digital pressure indicators. The gas inlet and outlet were also equipped with digital thermometers to monitor the temperatures. It is important to know both inlet and outlet temperatures of the gas stream in order to check any cooling effect, which might result into a change in the volumetric gas flow rate. CO_2 concentration in the feed and outlet gas streams of the contactor was measured using Maihak Infrared CO_2 analyzer of different ranges depending on gas composition (0–5%, 0–15%). The experiments were carried out using mixed streams of N_2 and CO_2. The samples of the gas stream were adjusted by dilution with calibrated amounts of N_2 in order to arrive at the concentration range required by the infrared analyzer. CO_2 absorption flux and average liquid outlet concentration were calculated by an overall mass balance over the reactor.

$$\langle J_{CO_2} \rangle = \frac{Q_{G,i}C_{G,i} - Q_{G,e}C_{G,e}}{A} \tag{7}$$

$$C_{L\,out} = \frac{Q_{G,i}C_{G,i} - Q_{G,e}C_{G,e}}{Q_L} \tag{8}$$

Since the infrared analyzer gave CO_2 concentration in terms of volume percentage, it was possible to calculate both the volumetric gas flow rate and the molar concentration of CO_2 by mass balance. In all experiments the gas flow rate was kept sufficiently low so that the outlet concentration of the CO_2 was significantly lower than the inlet conditions. The solubility of CO_2 in water in terms of distribution coefficient 'm' at experimental conditions was taken from Versteeg and van Swaaij [8].

4. Results and discussions

4.1. Absorption experiments

Absorption experiments were carried out to study the influence of various operating parameters such as gas-side residence time, liquid velocity and CO_2 partial pressure on the module performance. In all experiments the gas residence time in the membrane module was kept such that a significant change in the gas phase concentration was obtained. Initial experiments were carried out using low concentration of CO_2 in the inlet gas stream and low rates of removals in order to avoid large changes in the volumetric gas flow rate due to absorption. Fig. 4 shows CO_2 concentrations in liquid and gas outlet for the absorption of 2.5% CO_2 in module II (inlet gas flow 0.65 l/min; 293 K) as a function of dimensionless variable a_{max}. The variable a_{max} was changed by changing the liquid flow rate through the module. It can be seen from the figure that the increase in liquid flow rate, which corresponds to decrease in the variable a_{max}, results in the decrease in both gas and liquid outlet concentration. The heat transfer (HT) analogy predictions of outlet gas and liquid concentrations are in good agreement with experimental results. It is important to note that in this case CO_2 removal was always less than 15%. Moreover, the changes in volumetric flow rate of the gas were very small (less than 0.5%) and were therefore allowed to be neglected. Thus for these process conditions the equations derived on the basis of heat transfer analogy can be used to estimate the performance of the module.

To analyze the effect of a change in the volumetric flow rate of the gas stream, experiments were carried out at relatively high removal rates and using a gas stream containing a higher CO_2 concentrations. Figs. 5 and 6 show CO_2 concentrations in liquid and gas outlet as a function of a_{max} for the absorption of 30% (inlet gas flow = 0.38 l/min) and 87.5% (inlet gas flow = 0.36 l/min) CO_2 in module II at 295 K, respectively. It can

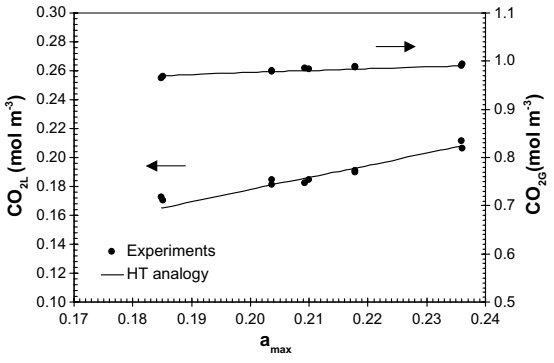

Fig. 4. CO_2 (2.5%) absorption in module II.

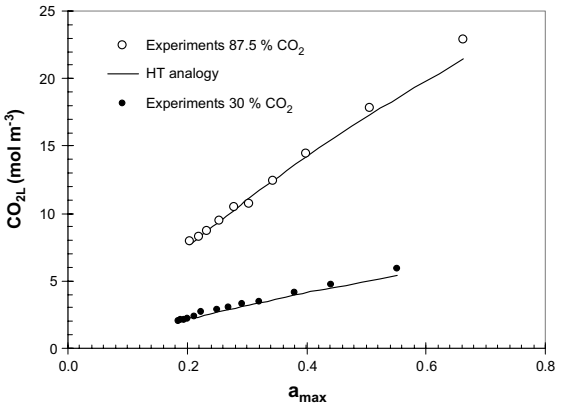

Fig. 5. Effect of a_{max} on the liquid outlet concentration for CO_2 absorption in module II.

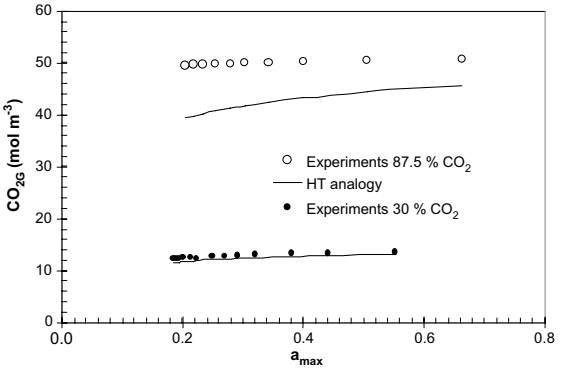

Fig. 6. Effect of a_{max} on the gas outlet concentration for CO_2 absorption in module II.

be seen from the graphs that the gas phase concentrations predicted by heat transfer (HT) analogies are lower than the experimental results and this deviation increases with the liquid velocity, i.e., with corresponding decrease in a_{max}. In general, the transfer of moles from gas phase to the liquid phase results into a decrease in the gas phase concentration as well as volumetric flow rate. However, the heat transfer analogy is derived for a constant volumetric flow rate and only takes into account the change in the solute concentration. As the solute concentration in the gas phase and the removal rate increases, the decrease in the volumetric flow rate for isobaric operation becomes more pronounced. In the present case, the percentage removal increases with the liquid velocity and hence the deviation in the prediction of the gas phase outlet concentration using heat transfer analogies also increases with the liquid velocity. Fig. 7 shows the percentage error in the gas outlet concentration as a function of percentage change in the gas-phase flow change for the case of 87.5% CO_2 absorption in

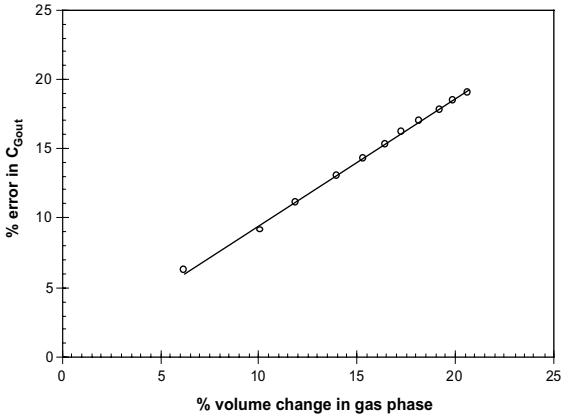

Fig. 7. Effect of gas flow-rate change on the prediction of gas outlet concentration.

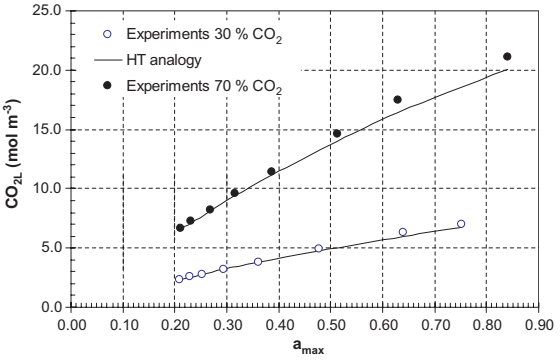

Fig. 8. Effect of a_{max} on the liquid outlet concentration for CO_2 absorption in module I.

module II. It can be seen from the figure that the error is proportional to the change in the volumetric flow of the compressible fluid.

Similar results were obtained for absorption of CO_2 using the larger module I at 295 K. The results are presented in Figs. 8 and 9. The gas flow rate during the experiment was kept constant at 16.1 l/min for the absorption of 70% CO_2 and at 13.3 l/min for the absorption of 30% CO_2. It can be seen from the figures that the case of 70% CO_2, the predictions of the gas outlet concentration based on the heat transfer (HT) analogy results into considerable deviations, whereas for the case of 30% CO_2 the predictions of the gas outlet concentration based in the heat transfer analogy matches well with experimental findings.

4.2. Analysis of cross-flow membrane contactor using heat transfer analogy

As discussed in Section 4.1, the heat transfer analogies can be used to predict the outlet concentrations of

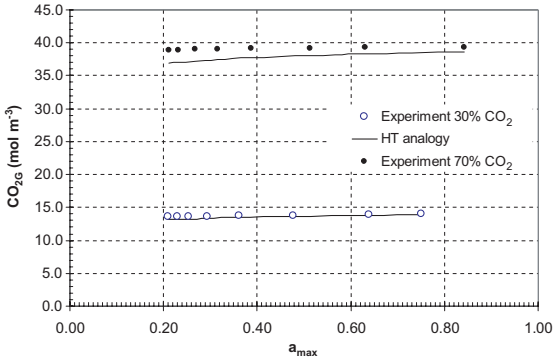

Fig. 9. Effect of a_{max} on the gas outlet concentration for CO_2 absorption in module I.

the cross-flow module when the change in the volumetric flow rate of the gas is very small and can be neglected. This necessary condition is achieved at low percentage removal and/or low solute concentrations. The heat transfer analogies with no mixing on the shell side can also be used to predict local concentration and driving force profiles within the limiting conditions. Fig. 10a,b, and c shows the dimensionless concentration profile on the fiber side, on the shell side and the dimensionless local driving force as a function of normalized position within the membrane gas–liquid contactor, respectively. Eqs. (A.19), (A.22) and (A.23) from Appendix A were used to calculate dimensionless concentration driving force, dimensionless gas and liquid concentrations, respectively.

As can be seen from Fig. 10a, when '*b*' increases the dimensionless liquid concentration Θ_L increases, i.e., local liquid concentration decreases (see the definition of dimensionless liquid concentration) in the direction of the gas flow. This is obvious since the absorption results into decreased gas concentration the direction of the gas flow thus reducing the mass transfer driving force. The dimensionless liquid concentration Θ_L decreases with increase in the direction of the liquid flow, i.e., liquid local concentration increases with '*a*' in the direction of liquid flow due to liquid saturation.

Fig. 10b indicates the dimensionless shell-side concentration profile of the module. The dimensionless shell-side solute concentration Θ_G decreases with increase in '*a*', i.e., local shell-side concentration increases with '*a*'. This is due the saturation of the liquid with the solute. The saturation of the liquid increases with '*a*' and hence amount of gas absorbed decreases with '*a*' thus increasing the local shell-side concentration. As expected Θ_G increases with increase in '*b*', i.e., local shell-side concentration decreases in direction of the gas flow.

Fig. 10c shows the dimensionless driving force as a function of the normalized module dimensions. It can be seen from the figure that as '*a*' increases, the local concentration driving force goes through maxima for

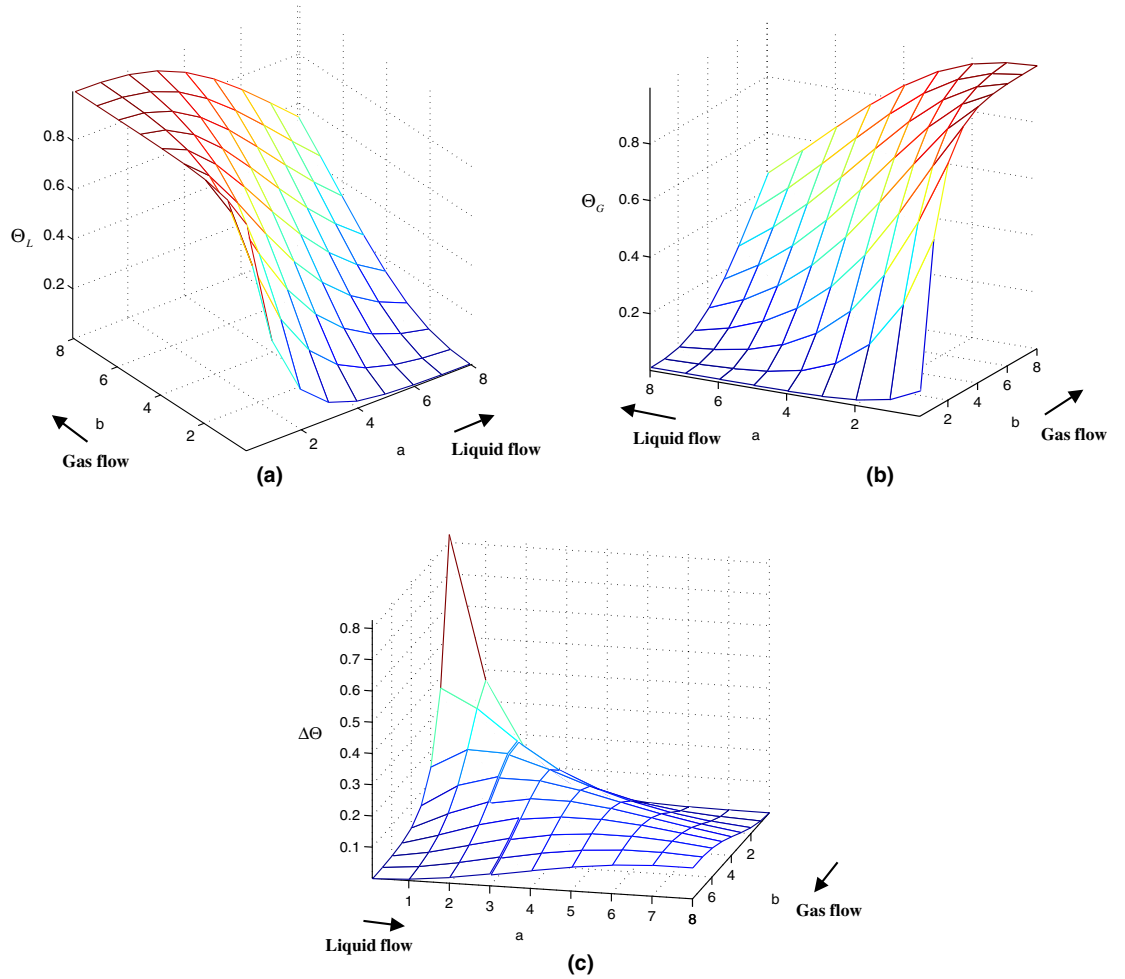

Fig. 10. (a) Local fiber-side concentration within the membrane contactor. (b) Local shell-side concentration within the membrane contactor. (c) Local concentration driving force within the membrane contactor.

given value of '*b*'. This driving force is at maximum in the corner of the module where the fresh feed gas first meets unloaded solvent which is represented by lowest value of '*a*' and '*b*'. Due to this high driving force the gas leaving that region will be depleted much faster in the solute concentration and thus driving force decreases sharply along the edge of liquid entrance ($a = 0$ and increasing b). Liquid flowing past this maximum driving force corner has increased solute concentration thus reducing the local driving force. Hence, less solute is absorbed by the liquid flowing through the fibers and eventually increasing again the gas phase concentration along '*a*' for given '*b*'. By this mechanism the maxima in driving force shifts its position from $a = 0$ and $b = 0$ towards the opposite corner.

These concentration and driving force profiles are useful in identifying less efficient/dead zone for mass transfer. The region near the liquid entrance and the gas exit has very low gas concentration and therefore is less efficient in the mass transfer process. In such cases, local reversal of the liquid flow direction or the installation of baffles perpendicular to gas flow to enhance the mass transfer in less efficient zones will improve the overall driving force.

5. Conclusion

In the present study, physical gas absorption in a rectangular cross-flow hollow fiber membrane gas liquid contactor is discussed in detail. Experiments were carried out to study the effect of various parameters such as gas and liquid flow rates, solute concentration in the feed stream on the performance of the rectangular cross-flow membrane gas–liquid contactors. The possibility of application of the cross-flow heat exchanger

analogy in the limiting cases to the cross-flow membrane gas–liquid contactor is explored. At low removal rates and/or low solute concentrations in the feed stream the experimental results match very well with the predictions of heat transfer analogies. Thus the cross-flow heat exchanger analogy can be used to predict concentration profiles and local driving force when percentage removals and solute concentrations in the feed stream are low resulting into low volumetric flow changes. This indicates that the mass-transfer performance of the cross-flow membrane contactors involving incompressible fluids such as liquid–liquid extraction can be directly predicted by the heat transfer analogy when the mass transfer is not aided by the chemical reactions. However, at higher percentages of removal and higher solute concentrations the change in the volumetric flow is significant and heat transfer analogy can no longer be used to predict the performance of the cross-flow gas–liquid membrane contactor. To predict the performance of the cross-flow membrane contactor in such cases a more detailed mathematical model should be used.

Acknowledgements

This research is part of the research program performed within the Centre for Separation Technology (CST), which is a co-operation between the Netherlands Organization for Applied Scientific Research (TNO) and the University of Twente. We acknowledge Benno Knaken and Wim Leppink for the construction of the experimental set-ups.

Appendix A. Analytical solutions for gas and liquid concentrations in a cross-flow hollow fiber membrane contactor

The mass balance Eqs. (1) and (2) can be solved analytically using new dimensionless variables as follows:

$$a = \frac{KY}{Q_L}x; \quad b = \frac{KX}{Q_G}y; \tag{A.1}$$

Using Eq. (A.1) in Eqs. (1) and (2)

$$\frac{\partial C_G}{\partial b} = -(mC_G - C_L) \tag{A.2}$$

$$\frac{\partial C_L}{\partial a} = (mC_G - C_L) \tag{A.3}$$

Differentiating Eq. (A.3) with '*b*' and using Eq. (A.2)

$$\frac{\partial^2 C_L}{\partial a\,\partial b} + m\frac{\partial C_L}{\partial a} + \frac{\partial C_L}{\partial b} = 0 \tag{A.4}$$

Similarly equation for C_G can be obtained by differential Eq. (A.2) with '*a*' and using Eq. (A.3)

$$\frac{\partial^2 C_G}{\partial a\,\partial b} + m\frac{\partial C_G}{\partial a} + \frac{\partial C_G}{\partial b} = 0 \tag{A.5}$$

The equation of the local concentration gradient can be obtained from Eqs. (A.4) and (A.5) and written as follows:

$$\frac{\partial^2 (mC_G - C_L)}{\partial a\,\partial b} + m\frac{\partial (mC_G - C_L)}{\partial a} + \frac{\partial (mC_G - C_L)}{\partial b} = 0 \tag{A.6}$$

In order to find a solution of Eq. (A.6) the procedure given by Hoffman [5] can be used. For the local concentration difference of the two fluids following assumption of the solution can be made.

$$(mC_G - C_L) = e^{-(a+mb)}.\Delta(a;b) \tag{A.7}$$

where $\Delta(a;b)$ is an unknown function of '*a*' and '*b*' which has to be determined. Using Eqs. (A.6) and (A.7) it can be shown that

$$\frac{\partial^2 \Delta(a;b)}{\partial a\,\partial b} = m\Delta(a;b) \tag{A.8}$$

For the function $\Delta(a;b)$, the following polynomial can be introduced.

$$\Delta(a;b) = A_0(ab)^0 + A_1(ab)^1 + A_2(ab)^2 + \cdots + A_N(ab)^N \tag{A.9}$$

Substituting Eq. (A.9) in (A.8) and comparing the resulting coefficients $(ab)^N$ on both side, the general term for the coefficient can be obtained and is given by Eq. (A.10)

$$A_N = \frac{m^N A_0}{(N!)^2} \tag{A.10}$$

The unknown function $\Delta(a;b)$ can be rewritten using Eqs. (A.10) and (A.9) as

$$\Delta(a;b) = A_0 \sum_{N=0}^{\infty} \frac{(mab)^N}{(N!)^2} \tag{A.11}$$

Using Eqs. (A.7) and (A.11), local concentration difference of the two fluids can be obtained.

$$(mC_G - C_L) = e^{-(a+mb)} A_0 \sum_{N=0}^{\infty} \frac{(mab)^N}{(N!)^2} \tag{A.12}$$

The constant A_0 can be determined from the boundary conditions.

$$x = 0; \rightarrow a = 0; \rightarrow C_G = C_{G,i} \tag{A.13}$$

$$y = 0; \rightarrow b = 0; \rightarrow C_L = C_{L,i} \tag{A.14}$$

From Eqs. (A.12)–(A.14);

$$(mC_{G,i} - C_{L,i}) = A_0 \tag{A.15}$$

Eq. (A.12) can be rewritten by using Eq. (A.15)

$$\frac{(mC_G - C_L)}{(mC_{G,i} - C_{L,i})} = e^{-(a+mb)} \sum_{N=0}^{\infty} \frac{(mab)^N}{(N!)^2} \tag{A.16}$$

With Eq. (A.16) the local concentration difference of the two fluids at any point of the contactor can be calculated. Eq. (A.16) also represents the ratio of local driving force to the maximum driving force. It is a function of the dimensionless variables 'a' and 'b'. For variable 'a' all values from $a = 0$ for $x = 0$ to $a = a_{\max}$ for $x = X$ are possible and also for variable 'b' all values from $b = 0$ for $y = 0$ to $b = b_{\max}$ for $y = Y$ are possible.

The local dimensionless concentrations can be defined as follows:

Local dimensionless gas phase (shell-side) concentration:

$$\Theta_{\mathrm{G}} = \frac{(mC_{\mathrm{G,i}} - mC_{\mathrm{G}})}{(mC_{\mathrm{G,i}} - C_{\mathrm{L,i}})} \tag{A.17}$$

Local dimensionless liquid phase (fiber-side) concentration:

$$\Theta_{\mathrm{L}} = \frac{(mC_{\mathrm{G,i}} - C_{\mathrm{L}})}{(mC_{\mathrm{G,i}} - C_{\mathrm{L,i}})} \tag{A.18}$$

Local concentration difference at any point of the contactor

$$\Delta\Theta = \Theta_{\mathrm{L}} - \Theta_{\mathrm{G}} = \frac{(mC_{\mathrm{G}} - C_{\mathrm{L}})}{(mC_{1,i} - C_{2,i})} = \mathrm{e}^{-(a+mb)} \sum_{N=0}^{\infty} \frac{(mab)^N}{(N!)^2} \tag{A.19}$$

The next step is to find out the local gas-phase concentration 'C_{G}' or corresponding dimensionless concentrations 'Θ_{G}'. Substituting Eq. (A.16) in (A.2) and integrating the equation along the constant 'a' line with upper limit 'b^*', it can be shown that,

$$\Theta_{\mathrm{G}} = m \int_0^{b^*} \mathrm{e}^{-(a+mb)} \sum_{N=0}^{\infty} \frac{(mab)^N}{(N!)^2} \partial b \tag{A.20}$$

Similarly the equation for the local liquid-phase 'C_{L}' or the corresponding dimensionless concentration 'Θ_{L}' can be obtained by substituting Eq. (A.16) in (A.3) and integrating the equation along the constant 'b' line with upper limit 'a^*', it can be shown that,

$$\Theta_{\mathrm{L}} = 1 - \int_0^{a^*} \mathrm{e}^{-(a+mb)} \sum_{N=0}^{\infty} \frac{(mab)^N}{(N!)^2} \partial a \tag{A.21}$$

The solution of the integral can be found easily. The final equations for the local concentrations are summarized below.

$$\Theta_{\mathrm{G}} = m\mathrm{e}^{-a} \sum_{N=0}^{\infty} \frac{a^N}{N!m} \left(1 - \mathrm{e}^{-mb^*} \sum_{N=0}^{N} \frac{(mb^*)^N}{N!}\right) \tag{A.22}$$

$$\Theta_{\mathrm{L}} = 1 - \mathrm{e}^{-mb} \sum_{N=0}^{\infty} \frac{(mb)^N}{N!} \left(1 - \mathrm{e}^{-a^*} \sum_{N=0}^{N} \frac{(a^*)^N}{N!}\right) \tag{A.23}$$

At the fiber-side outlet, where $x = X$ or $a^* = a^*_{\max}$, the local concentration 'C_{L}' or corresponding dimensionless concentration 'Θ_{L}' is only function of 'b'. Since all streamlines mix at outlet, the mean outlet concentration is given by

$$\Theta_{\mathrm{L}\,xm} = \frac{(mC_{\mathrm{G},i} - C_{\mathrm{L}xm})}{(mC_{\mathrm{G},i} - C_{\mathrm{L},i})} = \frac{1}{b^*} \int_0^{b^*} \Theta_{\mathrm{L}}\, \partial b \tag{A.24}$$

Using Eq. (A.23) one can obtain the final solution.

$$\Theta_{\mathrm{L}\,xm} = 1 - \frac{1}{mb^*} \sum_{N=0}^{\infty} \left(1 - \mathrm{e}^{-mb^*} \sum_{N=0}^{N} \frac{(mb^*)^N}{N!}\right) \times \left(1 - \mathrm{e}^{-a^*} \sum_{N=0}^{N} \frac{(a^*)^N}{N!}\right) \tag{A.25}$$

Similarly at the shell-side outlet, where $y = Y$ or $b^* = b^*_{\max}$, the local concentration 'C_{G}' or corresponding dimensionless concentration 'Θ_{G}' is only function of 'a'. The mean outlet concentration for shell-side flow is given by

$$\Theta_{\mathrm{G}\,xm} = \frac{(mC_{\mathrm{G},i} - mC_{\mathrm{G}xm})}{(mC_{\mathrm{G},i} - C_{\mathrm{L},i})} = \frac{1}{a^*} \int_0^{a^*} \Theta_{\mathrm{G}}\, \partial a \tag{A.26}$$

The using Eq. (A.22) final solution for Θ_{G} is given by

$$\Theta_{\mathrm{G}\,xm} = \frac{1}{a^*} \sum_{N=0}^{\infty} \left(1 - \mathrm{e}^{-a^*} \sum_{N=0}^{N} \frac{(a^*)^N}{N!}\right) \times \left(1 - \mathrm{e}^{-mb^*} \sum_{N=0}^{N} \frac{(mb^*)^N}{N!}\right) \tag{A.27}$$

The mean effective concentration difference $(\Delta C)_{\mathrm{xm}}$ can be obtained by integrating the local concentration difference over the entire area of module.

$$\Delta\Theta_{\mathrm{xm}} = \frac{(\Delta C)_{xm}}{(mC_{\mathrm{G},i} - C_{\mathrm{L},i})} = \frac{1}{a^*b^*} \int_0^{a^*} \int_0^{b^*} \Delta\Theta\, \partial a\, \partial b \tag{A.28}$$

Using Eq. (A.19) final solution can be obtained and is given by Eq. (A.29)

$$\Delta\Theta_{\mathrm{xm}} = \frac{1}{a^*mb^*} \sum_{N=0}^{\infty} \left(1 - \mathrm{e}^{-a^*} \sum_{N=0}^{N} \frac{(a^*)^N}{N!}\right) \times \left(1 - \mathrm{e}^{-mb^*} \sum_{N=0}^{N} \frac{(mb^*)^N}{N!}\right) \tag{A.29}$$

References

[1] S.R. Wickramasinghe, M.J. Semmens, E.L. Cussler, Mass transfer in various hollow fiber geometries, J. Membr. Sci. 69 (1992) 235–250.

[2] A.E. Jansen, R. Klaassen, P.H.M. Feron, J.H. Hanemaaijer, B.P. ter Meulen, Membrane gas absorption processes in

environmental applications, in: J.G. Crespo, K.W. Boddeker (Eds.), Membrane Processes in Separation and Purification, Kluwer Academic Publishers, Dordrecht, 1994, pp. 343–356.

[3] W. Nusselt, Der warmeubergang im kreuzstorm, Zeitschrift des Vereines deutscher Ingenieur 55 (1911) 2021–2024.

[4] D.M. Smith, Mean temperature difference in cross-flow, Engineering 138 (1934) 479–482, 606–607.

[5] Hoffman, Theoretical solution for cross-flow heat exchanger, Heat Mass Transfer 36 (2000) 127–133.

[6] V.Y. Dindore, A.H.G. Cents, D.W.F. Brilman, G.F. Versteeg, Shell-side dispersion coefficients in a rectangular cross-flow hollow fiber membrane module, Chem. Eng. Res. Des. 83 (A3) (2005) 317–325.

[7] V.Y. Dindore, D.W.F. Brilman, F.H. Geuzebroek, G.F. Versteeg, Membrane-solvent selection for CO_2 removal using membrane gas–liquid contactors, Separ. Purif. Technol. 40 (2004) 133–145.

[8] G.F. Versteeg, W.P.M. van Swaaij, Solubility and diffusivity of acid gases in aqueous alkanolamine solutions, J. Chem. Eng. Data 33 (1988) 29–34.